Meteorological overview and verification of HYSPLIT and AAQFS dust forecasts for the duststorm of 22-24 October 2002

A.G. Wain[1], S. Lee[2], G. A. Mills[1], G. D. Hess[1], M. E. Cope[2] and N. Tindale[3]

[1]Bureau of Meteorology Research Centre, Australia
[2]CSIRO Atmospheric Research, Australia
[3]University of the Sunshine Coast, Australia

(Manuscript received June 2005; revised January 2006)

The large-scale dust event that was observed in much of central and eastern Australia over the period 22-24 October 2002 was one of the largest experienced in Australia in recent decades. Its large scale, and the high quality observations of the storm from a variety of observing platforms, provided the opportunity to verify forecasts of the dust transport during this event from two particulate transport models.

Analyses from the Bureau of Meteorology's Limited Area Prediction Scheme were used as a diagnostic tool to describe the synoptic dynamics that allowed strong winds from aloft to reach the surface, where gusts > 40 kn persisting through the nocturnal hours were observed in post-frontal winds. Comparisons of output from both transport models with observations from satellite and ground-based platforms are presented at four times over a 36-hour period during the duststorms' transit of mainland Australia. It is demonstrated that the performance of forecasts from both transport models in predicting the position of the dust front was quite good. However, it is shown that the forecasts are very sensitive to the land-surface specification that delineates potential source regions for the dust, and these data require further development before operational dust forecasting using these models could be relied upon.

Introduction

On 22 October 2002, a frontal system entered South Australia (SA), and over the next 36 hours associated strong winds raised dust over a wide region of eastern Australia, from central SA, extending eastwards and northeastwards through SA, New South Wales (NSW) and Queensland (Qld) (see Figs 1 and 2 for locations referred to in the text). Forty-six Bureau of Meteorology synoptic observing stations reported dust during 22-23 October. McTainsh et al. (2005) state that, based on satellite imagery, the dust cloud

Corresponding author address: Dr A. Wain, Bureau of meteorology Research Centre, GPO Box 1289, Melbourne, Vic. 3001, Australia.
Email: a.wain@bom.gov.au

Fig. 1 Locality diagram.

Fig. 2 Rainfall percentages for the eight-month period ending 31 October 2002.

was over 2400 km long and 400 km wide, and visibility was markedly reduced over wide areas of eastern Australia on 23 October, including at both Brisbane and Sydney airports.

Chan et al. (2005) reported that the 24-hour average concentrations of particulate matter having an equivalent aerodynamic diameter less than or equal to 10 micrometres (PM10) recorded in Brisbane during this event were more than three times the level of national ambient air quality standard of 50 μg m^{-3} while those in Mackay (Qld) were almost 10 times greater than the standard. An extended drought had created conditions conducive to aeolian dust transport, with much of Australia experiencing a serious rainfall deficiency (Fig. 2). Records of three-hourly synoptic data for Woomera show dust or haze were recorded in over 25 per cent of the observations (64/248) for October 2002. Mildura recorded dust or haze in just over 12 per cent of observations with dust storms occurring on the 16, 18 and 23 October 2002.

The scale and duration of this dust event enabled good satellite observations of the event as well, from a variety of satellite-based instruments. These data in turn afforded an excellent opportunity to validate the ability of the Australian Air Quality Forecasting System (AAQFS) (Cope et al. 2004) and the HYbrid Single-Particle Lagrangian Integrated Trajectory (HYSPLIT) (Draxler and Hess 1998) models to forecast the development of these potentially disruptive natural events. Both models used meteorological input generated by the Bureau of Meteorology's Limited Area Prediction System (LAPS) (Puri et al. 1998). Forecast comparisons are made with visible satellite images from both the GMS-5 geostationary satellite and the MODerate-resolution Imaging Spectroradiometer (MODIS) carried on the Terra and Aqua polar-orbiting satellites, and with ground-based observations.

This paper is presented in two parts. The first provides an overview of the synoptic situation during the passage of the cold front across eastern Australia and discusses the features of the meteorology of the event that appear relevant to the resulting duststorm. The second section examines the ability of the AAQFS and HYSPLIT models to forecast the movement of the dust front, comparing forecasts from the two systems with satellite imagery and surface observations at a number of lead-times, and demonstrates the sensitivity of the forecasts to surface land-surface specification.

Synoptic overview

The synoptic overview covers the period 1800 UTC 21 October 2002 to 0000 UTC 23 October 2002, and uses the 0.375° latitude/longitude grid of LAPS (Puri et al. 1998) initialised numerical analyses, as these have been shown in many case studies (e.g. Mills 1997) to be dynamically balanced from the data assimilation cycle while fitting the observations well, and thus provide powerful diagnostic datasets with which to describe the synoptic-dynamics of the atmosphere.

The sequence of LAPS mean sea-level pressure (MSLP) analyses is shown in Fig. 3, with the wind field from the model's 0.9943 sigma level (approx 30 m) overlain. This level is anecdotally considered by Australian forecasters to provide a good indication of the observed 10 m winds, and so is used here for that

Fig. 3 **Mean sea-level pressure analyses and wind barbs at ~30 m from the operational LAPS analyses at six-hourly intervals from 1800 UTC 21 to 0000 UTC 23 October 2002. The contour interval for pressure is 2 hPa, and the wind barbs have their usual meteorological meaning, with a long barb representing 10 kn. The line shows the location of the cross-sections in Figs 5 and 6.**

(a)

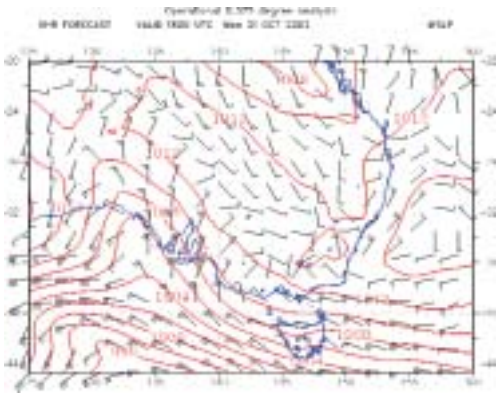

(b)

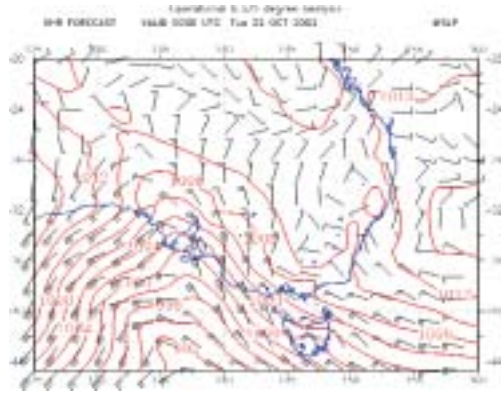

(c)

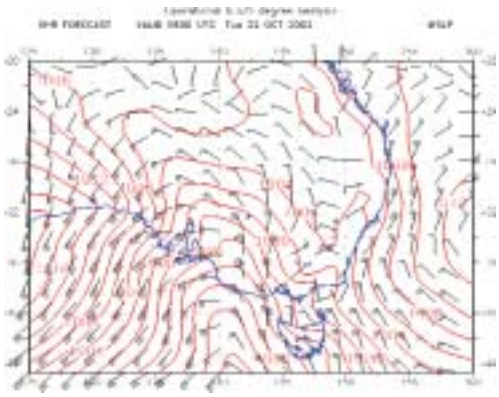

(d)

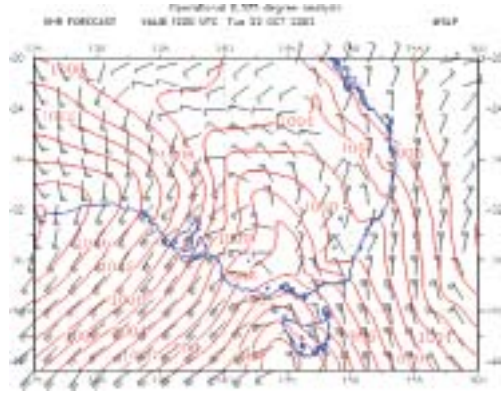

(e)

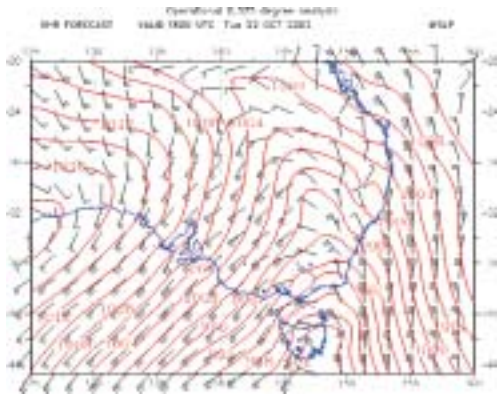

(f)

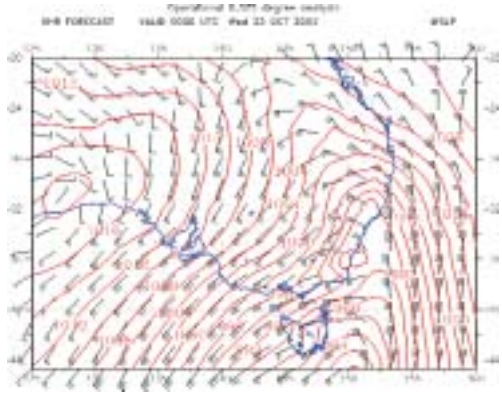

reason. At 1800 UTC 21 October (Fig. 3(a)) a trough of low pressure was crossing into the western part of SA, with a sharp southern ocean trough moving rapidly into the plot area from the southwest. The pressure gradient both east and west of this trough increased rapidly, and by 0000 UTC 22 October (Fig. 3(b)) low-level northerly winds exceeding 30 kn are seen over the southeast of SA, and a large area of southwesterly winds above 30-35 kn west of the trough over the Great Australian Bight. During the daylight hours of 22 October the surface trough moved rapidly through SA and by 1200 UTC 22 October (Fig. 3(d)) extended from central Victoria through NSW, and was just reaching the southwest corner of Queensland. Pressures rose very rapidly west of the trough (seen in the isallobar field in Fig. 4) and as a result of this strong pressure gradient most of SA experienced 30-35 kn winds following the trough passage. These strong winds moved into NSW and Queensland in the wake of the trough. A consequence of these rapid pressure rises, and the very strong isallobaric gradient stretching along the length of the front (Fig. 4), is the marked ageostrophy of these post-frontal winds – the winds are directed across the isobars towards low pressure (Figs 3(c),(d),(e)), indicating rapid accelerations in the low-level flow with a time-scale much shorter than that required for the atmosphere to achieve geostrophic balance.

The upper-level flow (Fig. 5) at 0000 and 1200 UTC 22 October 2002 shows a mobile mid-latitude trough moving eastwards into southeastern Australia with two distinct jet streaks, one near the apex of the trough that moved northeastwards into northern NSW and southern Queensland, and a second jet streak on the western flank of the trough.

Surface observations through SA show strong and gusty winds before the change, but also show even stronger winds for a sustained period after the frontal passage, with stations from Eyre Peninsula to the far northeast of SA reporting a sustained period of mean wind speed above 25 kn and with gusts above 45 kn in the post-frontal air. Examples are shown in Fig. 6 for Wudinna, Woomera, Leigh Creek, Marree and Moomba (Fig. 1), close to the line from central Eyre Peninsula to the far northeast of SA shown in Fig. 3. There are two other interesting features of these time-sequences of the observations. One is the extremely low humidities in the pre-frontal airmass – dew-point values below –10°C, indicating relative humidities of less than 5 per cent were widespread. Combined with the strong winds, the high temperatures and the pre-existing drought (Fig. 2), this would have contributed to surface dust being extremely dry. The second feature is the fact that the strong winds and gustiness persisted well into the night in the northeast of SA, con-

Fig. 4 Field of six-hour isallobar (mean sea-level pressure change) between 0600 and 1200 UTC 22 October 2002. Contour interval is 1 hPa, and areas of pressure fall are dashed.

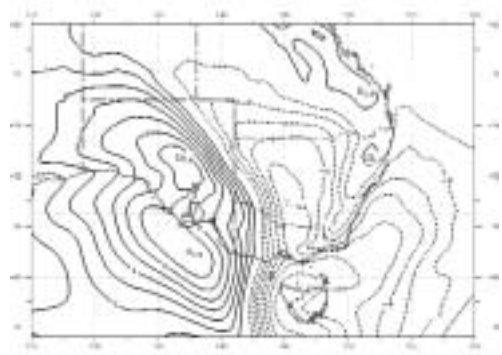

Fig. 5 300 hPa height/wind analyses at 0000 UTC and 1200 UTC 22 October 2002. Height contours (heavy) are at intervals of 60 gpm, and isotachs are shaded at 40 and 50 m s^{-1}.

(a)

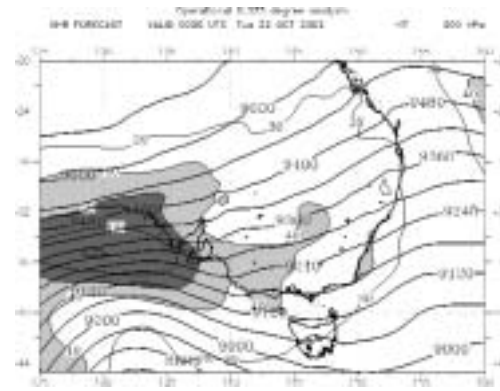

(b)

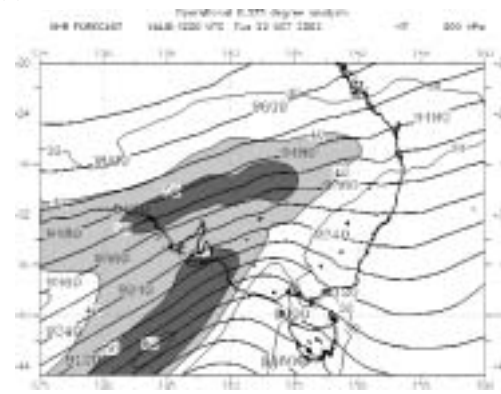

Fig. 6 **Meteograms at Wudinna (YWUD), Woomera (YPWR), Leigh Creek (YLEC) and Moomba (YOOM). In the upper panel of each pair, direction is black, with the ordinate values on the right, while speed (red) and gust (green) share the left-hand ordinate scaling. In the lower panels temperature is red and dew-point green, with absolute values offset.**

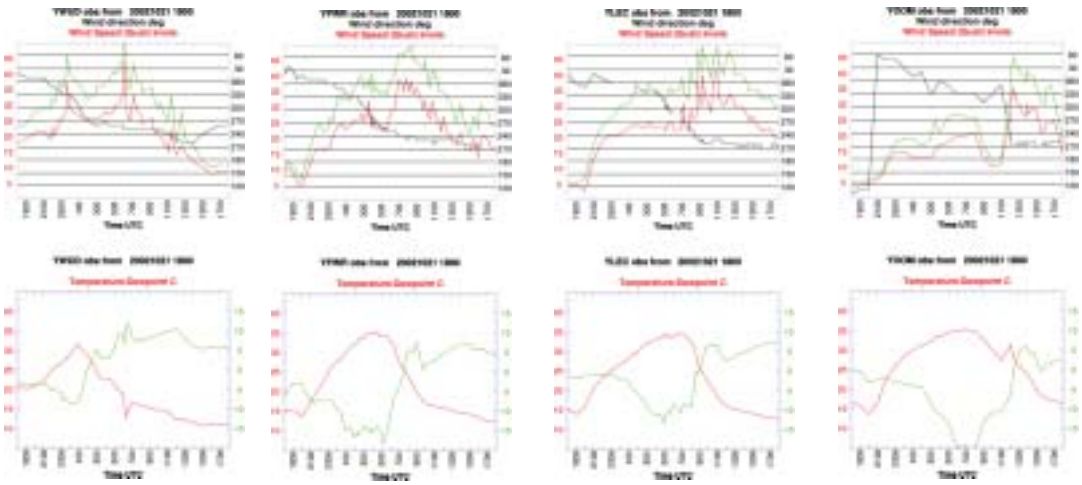

trary to the normal expectation that both post-frontal and nocturnal stability increases would reduce the wind speed and gustiness.

A vertical cross-section from southwest of SA through Eyre Peninsula to south-central Queensland (Fig. 3(c) shows the location), at 0000 UTC 22 October (Fig. 7(a)) shows a shallow mixed layer (weak vertical potential temperature gradient) over the interior of the continent, and a deep layer of steeply sloping isentropes extending southwestwards from near the Eyre Peninsula coastline. The strong jet stream extending from the upper troposphere down the sloping baroclinic zone is very evident. This is clearly a highly baroclinic system extending through most of the depth of the troposphere. The same cross-section six hours later (Fig. 7(b)) shows the front (defined as the first isentrope to intersect the ground west of the mixed layer, and consistent with Hewson's (1998) definition of the frontal location as the warm edge of the zone of strongest thermal gradient) to have moved well into SA. Notably the isentropes have become vertically oriented at the nose of the front, probably as a result of diabatic heating being concentrated below the frontal inversion after the frontal passage. This does mean that for a considerable distance to the west of the initial frontal passage the mixed layer extends from the surface to some 750 hPa, where winds are shown to be around 25 m s^{-1}. With the low static stability in this layer, these strong winds can be realised as gusts at the surface, and the wind speeds near the top of this mixed layer are consistent with the gust speeds observed (Fig. 6). The marked pressure rises seen in Figs 3 and 4 are the hydrostatic response to the deep, strong cold advection in the post-frontal zone.

At 1200 UTC 22 October 2002, the cross-section (Fig. 8) shows that while a surface inversion is beginning to form ahead of the front, a combination of diabatic heating and (probably) mechanical turbulence is acting to maintain a post-frontal mixed layer, and thus to allow the gustiness to continue well after sunset, again consistent with the observations (Fig. 6). Also shown in Fig. 8 is a representation of the cross-frontal vertical circulation associated with the front, and it is evident that there is a very strong descending branch to the rear of the front, with one cell associated with the surface front, and one in the mid-troposphere associated with the deep baroclinic wave. This downward motion would contribute to downward momentum transfer, and the tongue of strong winds extending nearly to the ground in the immediate post-frontal zone is co-located with this descent zone.

Deep, mobile fronts have been shown to be associated with strong post-frontal winds as seen in the case of the Ash Wednesday fires (Mills 2005). That analysis showed that the cold front associated with the well-documented Melbourne duststorm of 8 February 1983 (Lourensz and Abe 1983) had a similar structure, as did the fronts associated with the duststorms through SA and NSW that preceded (16

Fig. 7 Cross-sections of potential temperature (black, contour interval 2 K) and wind speed (dashed red, contour interval 5 m s^{-1}) along a southwest-northeast section through Eyre Peninsula at 0000 (top) and 0600 UTC 22 October (bottom). Right-hand axis shows height in hPa.

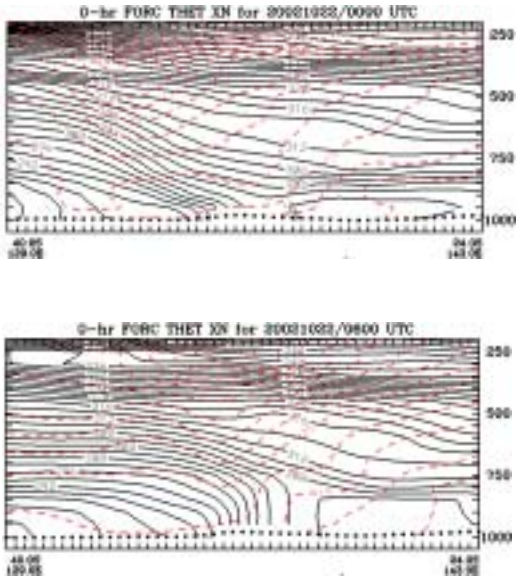

October and 18 October 2002) and followed (12 November and 29 November 2002) the 22 October event. It is the depth of the cool air associated with these fronts that leads to large pressure rises and thus strong post-frontal pressure gradients. Apart from the necessity for the drought precursor (dry bare soil that can be lifted) this is a significant meteorological ingredient, and may indeed be a necessary ingredient, in these widespread dust events. A study by Pauley et al. (1996) describes a duststorm in California. The synoptic environment of their storm had many similar ingredients to that of the 22 October case over Australia, with a fast-moving front, strong isallobaric gradients, strong and highly ageostrophic winds on the cool-air side of the front, mid and lower tropospheric descent in the strong wind zone, and a near-surface destabilisation mechanism that facilitated the extension of the strong winds to the surface.

The transport models

The AAQFS consists of five major components: a numerical weather prediction (NWP) system (LAPS), an emissions inventory module (EIM), a

Fig. 8 Upper panel - cross-section of potential temperature (black, contour interval 2 K) and wind speed (dashed red, contour interval 5 m s^{-1}) along a southwest-northeast section through Eyre Peninsula at 1200 UTC 22 October. Right-hand axis shows height in hPa. The lower panel shows vectors of the component of the ageostrophic wind in the plane of the cross-section versus the vertical motion. The contours show the vertical motion, with ascent areas dashed, and a contour interval of 10 hPa h^{-1}.

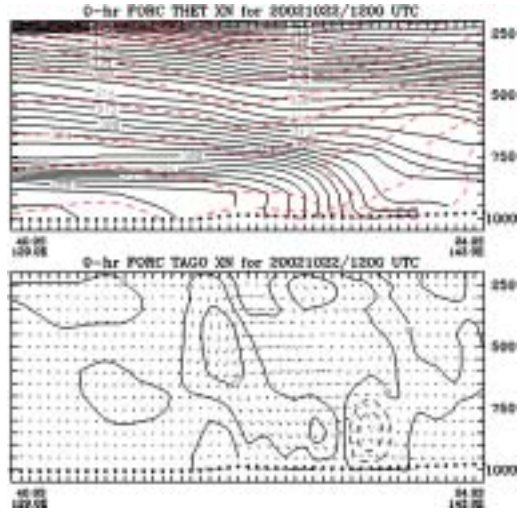

chemical transport module (CTM) for air quality modelling, an evaluation module and a data archiving and display module (Cope et al. 2004). For the AAQFS dust forecasting applications described in this paper the photochemistry and the emissions inventory for gaseous and particle species other than wind-blown dust are deactivated. The LAPS model (Puri et al. 1998) is run at 0.125° horizontal resolution to provide the meteorological input covering all of Australia. However, to reduce computation time the resolution of the meteorological input data is decreased to 0.25° prior to use by AAQFS. The LAPS model has 29 vertical levels with 11 levels within the lowest approximately 1500 m. Comprehensive numerical and physical packages are included and recent work has paid special attention to the treatment of near-surface processes.

The dust emissions module of AAQFS follows Lu and Shao (2001) and is based on the dust volume removed by saltation bombardment, considered to be the main mechanism for dust emission. The model first calculates horizontal sand flux by saltation for

each particle-size class based on Owen's saltation flux equations, and then calculates the vertical dust flux arising as a result of the saltation bombardment. The emissions are governed by (a) the characteristics of the soil: soil type, density, compactness and soil moisture content, (b) the characteristics of land surface: vegetation cover and non-erodible elements (rocks, lakes), and (c) the climate and weather conditions: precipitation, evaporation and wind speed. Lu and Shao's (2001) soil classification scheme, where there are 20 erodible types of soil grouped into eight units according to the availability of soil particle size distributions (PSDs) and chemical similarities was adopted. Eight PSDs of typical Australian soil types were provided by Dr Grant McTainsh of Griffith University. The smallest resolvable particle size is 2 μm and largest 1159 μm. A monthly leaf area index climatology and a 32 member vegetation type classification for Australia were obtained from Dr Dean Graetz of CSIRO Atmospheric Research.

HYSPLIT (Draxler and Hess 1998) uses a hybrid approach to modelling pollutant transport. Calculations of advection and dispersion are made in a Lagrangian framework following the path of the pollutant, in this case dust. The concentration calculations are made in an Eulerian framework, i.e. on a fixed grid. The PM10 dust emission algorithm described by Draxler et al. (2001) was used, with the dust flux calculated using the equation $F = 0.01u_*^4$ (Westphal et al. 1987) and dust emissions, up to a maximum value of 1 mg m^{-2} s^{-1}, occur when the friction velocity exceeds a specified threshold velocity.

For this event two different methods of specifying potential dust sources were considered. The first utilised the global land-use scheme contained within the HYSPLIT code and defined only those areas considered desert as possible source regions. This scheme has eleven categories and is based upon a 1° grid. Dust emissions for the desert land-use category have been adjusted to correspond to Kuwait's 'active sand sheet' where the emission fluxes were based on digital soil characteristics. The other method followed Loewe (1943) who identified areas of high duststorm frequency in Australia. This five-year (1938-1942) dataset represented another particularly dry period, and the area identified by Loewe also largely coincided with regions which had received less than 40 per cent of mean annual rainfall in the 12 months preceding October 2002 (Fig. 2). Source points were designated at 1° intervals within the area Loewe identified as having the greatest duststorm frequency. In addition to the source region for the Loewe high duststorm frequency three source points were placed on the northwest coast of Australia, based on studies of McTainsh and Pitblado (1987).

Only 12 points considered desert in the HYSPLIT default land-use scheme were coincident with the source areas identified by Loewe. This is not necessarily inconsistent with other findings that show areas of highest duststorm frequency away from the recognised desert regions (e.g. McTainsh and Pitblado 1987; Middleton 1984). Indeed, hyper-arid regions with annual rainfall of less than 100 mm experience a reduction in duststorm frequency with decreasing precipitation (Goudie 1983, p.515). With either land specification, the HYSPLIT model emits dust and transport begins from that location when the wind speed exceeds a specified threshold velocity at the source height (assumed to be 1 m). The time the dust remains in suspension is determined by the mean particle size (3 mm) the particle density (2.5 g cm^{-3}) and shape (assumed to be spherical), which are used to calculate the gravitational settling rate of the particles. In all forecasts HYSPLIT utilised the 0.125° meso-LAPS meteorological data at its full resolution.

Draxler (2004) used HYSPLIT and meteorological data from a global model to simulate this dust event, using the desert land use category. He compared his results with the 24-hour averaged Aerosol Index (AI) calculated from Total Ozone Mapping Spectrometer (TOMS) data. On 22 October the forecast dust was significantly west of the position indicated by the AI but by 24 October there was excellent agreement in eastern Australian and the Tasman Sea. However, the forecast also produced large concentrations of dust in regions where none was observed.

Verification data

Ground-based observations of dust have been used previously in studies of long-range transport of large-scale duststorms in China (Merrill et al. 1989) as well as in Australia (Middleton 1984; McTainsh and Pitblado 1987). More recently, McTainsh (1998) has developed the concept of a 'duststorm index', based on a 32-year meteorological record from 72 well-established Australian Bureau of Meteorology (BoM) stations to obtain wind erosion event data. Through the use of synoptic observations of dust, the occurrence and progress of large duststorms can be seen and tracked across the continent. Dust observations from BoM weather stations and observers were also used in our study to create maps of dust activity over time. From the three-hourly synoptic observations, the codes for duststorms (codes 09, 30-35) haze (05), and local blowing dust (codes 07 and 08), when available, were used to plot the passage of the duststorm across the south, southeast and east of Australia. There were some isolated observations of dust, or the

absence of dust, that were not consistent with the general passage of the duststorm, and these observations were removed from the dataset.

The initial report of dust on 22 October 2002 was from SA where Woomera Aerodrome reported dust continuously from 12.02 pm until 5.15 pm (0232-0745 UTC) (local time used unless noted). Visibility reached a minimum of 200 metres between 4.45 and 5.15 pm. There were no visual observations of dust reported during the night of 22 October, but at daybreak (0600 report) on the 23rd (2000 UTC on 22nd) severe duststorm activity was reported in the southwest Queensland/NSW border region. The 0900 (2300 UTC) reports show the duststorm activity spreading progressively eastwards into Queensland and NSW, reaching the coast by 1800 (0800 UTC) as illustrated by the reports from Brisbane at that time (at 1745 Brisbane Airport reported a visibility of 1500 m). Additional reports of dust continued in Queensland through 0900 to 1800 the following day, 24 October.

Satellite observations of dust provide good spatial and temporal resolution of the passage of large duststorms over long distances. Geostationary satellites (GMS-5 and GOES-9) provide frequent position updates although the spatial resolution is limited. Instruments carried on board polar-orbiting satellites (NOAA-AVHRR, MODIS) provide higher resolution imagery, but can only give twice-daily observations. Visual channel observations from both geostationary and orbiting satellites were utilised to provide verification in this study. As an example, Fig. 9 shows the visible GMS-5 satellite image at 2030 UTC 22 October 2002, together with locations where dust was reported in the synoptic observations (red dots) and the position of the cold front and the pre-frontal trough from the National Meteorological and Oceanographic Centre analysis for the time. To aid in interpretation the visible outline of the dust plume has been drawn as a polygon.

Fig. 9 Visible dust outlined (yellow) on rectified GMS satellite image using ArcGIS. The image is taken at 2030 UTC 22 October 2002. The blue and brown lines show the position of the cold front and pre-frontal trough as analysed by the National Meteorological and Oceanographic Centre, and the red dots mark locations where the synoptic observations reported dust.

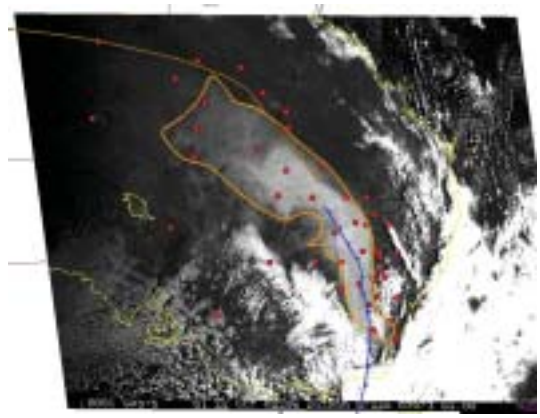

Forecast model configurations

HYSPLIT forecasts were created for the dust event of 22-24 October using a range of threshold velocities for both source area schemes and the results compared with the position of the dust front observed in satellite images. The experimentation with threshold velocity, the speed required for a dust/sand particle to be entrained by the wind, was necessary because its value has been found to vary according to the local arrangement of topography, geology, and meteorology and, as noted previously, the dust algorithm for HYSPLIT was developed using data from Kuwait. This tuning of HYSPLIT took place immediately after the 22-24 October dust event and in the absence of any prior validation of the dust generation code for Australian conditions. The subsequent comparison with AAQFS utilised data from the same event. As such the results obtained must be considered indicative until opportunities for further validation occur.

Helgren and Prospero (1987) found the average minimum wind speed associated with a dust event in the Western Sahara to be 8.2 m s^{-1} and the mean speed for all events to be 10.5 m s^{-1}. Nickling (1983) observed transport of sediments at mean wind speeds within the range of 4-12.7 m s^{-1}. Given this uncertainty, threshold velocities from 6-12 m s^{-1} were trialled to ascertain which value produced the most representative forecast result, and a comparison of several of these forecasts is shown in Fig. 10. Higher threshold velocities naturally resulted in a lesser area of dust, while lower threshold velocities sometimes produced dust in unlikely places, particularly when using the desert land-use scheme (which has a gridpoint in western Tasmania - the only area in Australia NOT to have duststorms (Middleton 1984)). Comparing the areas of forecast dust in Fig. 10 with the observed dust distribution at that time (Fig. 9), it was decided to use a threshold velocity of 10 m s^{-1} for subsequent HYSPLIT forecasts.

Fig. 10 **HYSPLIT forecasts using various threshold velocities between 7 and 10 m s^{-1} are shown based at 0000 UTC 22 October 2002, and valid at 2030 UTC 22 October 2002. The higher speed thresholds overlay the lower as forecast areas decrease with increasing threshold velocity. Forecast contours are in g m^{-3}. (A value of 10^{-4} g m^{-3} = 100 μg m^{-3}.)**

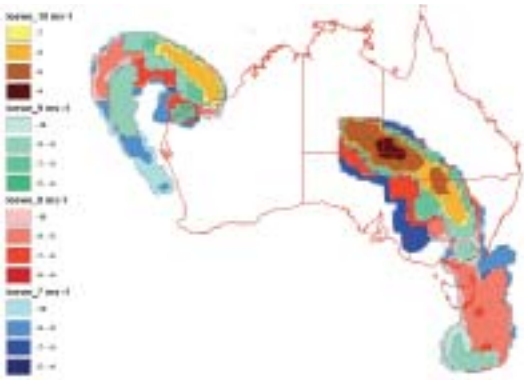

Fig. 11 **Comparison of HYSPLIT forecasts based at 0000 UTC 22 October 2002, and valid at 2030 UTC 22 October 2002 using a threshold velocity of 10 m s^{-1}, and the Loewe and default (desert) land-use schemes.**

Figure 11 shows a comparison of the HYSPLIT forecasts using the two different source region specifications. The pink shaded areas depict results using the desert land-use scheme; the green shading shows forecast raised dust concentration using the Loewe sources. The actual position of the dust plume visible in the satellite image (Fig. 9) is shown as an outline. This matches quite well with the analysed position of the cold front and also with the Loewe forecast. Overall, those simulations that used the Loewe source areas modelled the position of the dust front much better, and so this specification, rather than the HYSPLIT desert land-use specification was used for the subsequent forecast intercomparison with AAQFS.

The forecasts to be shown begin at 0000 UTC on 22 October 2002, with the NWP data updated at 12-hourly intervals. Four comparisons between AAQFS and HYSPLIT results are presented, with forecast durations of 15, 20, 24 and 32 hours. All were chosen because of the availability of clear satellite imagery showing the location of the dust front and are presented in chronological order. AAQFS forecasts display PM60 values in μg m^{-3}. HYSPLIT forecasts display exponential values of PM10 in g m^{-3}. A displayed value of –7 represents a concentration equal to 10^{-7} g m^{-3} or 0.1 μg m^{-3}.

Forecasts valid 1500 UTC 22 October 2002 (0100 EST 23 October)

The satellite data used for this comparison came from the MODIS instrument on the Terra satellite. A ‘split window’ analysis was applied to the data by Fred Prata of CSIRO Atmospheric Research (personal communication 2002) to obtain the dust area shown in Fig. 12. Approximately 12 hours after the initial report of dust by the observer at Woomera the plume visible in the satellite image extends along a line extending roughly from Birdsville to Cobar, approximately 1000 km long by 300 km across (Fig. 12). The analysed position of the cold front in this case has been interpolated between the positions shown in the 1200 UTC and 1800 UTC MSLP analyses. The eastern (leading) edge of the dust plume outline aligns well with the analysed position of the front, although perhaps lags a little behind it. The HYSPLIT forecast for this time lags some 130 km behind the observed position, although the extent and shape of the forecast dust plume matches that of the observed plume quite well. The AAQFS forecast matches the leading edge of the dust front well, but shows a much larger area of dust than is seen in the satellite imagery, with a forecast maximum concentration in northeastern SA which is not particularly evident in the satellite image. A second area of high concentration northeast of Kalgoorlie, in the Great Victoria Desert, is also not visible in the satellite data.

Fig. 12 **HYSPLIT and AAQFS dust forecasts for the forecast based at 0000 UTC 22 October 2002, and valid at 1500 UTC 22 October 2002. The positions of the cold front (blue and the pre-frontal trough (red) from the NMOC analyses are shown, together with the outline of the dust plume from the MODIS satellite imagery in yellow. Contour values are given in μg m^{-3}.**

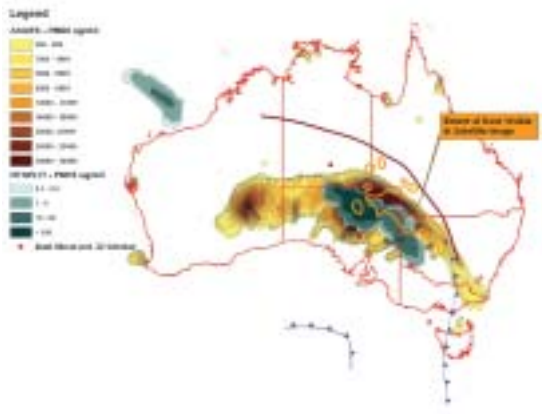

Fig. 13 **HYSPLIT and AAQFS dust forecasts for the forecast based at 0000 UTC 22 October 2002, and valid at 2000 UTC 22 October 2002. The positions of the cold front (blue and the pre-frontal trough (red) from the NMOC analyses are shown, together with the outline of the dust plume from the GMS-5 satellite imagery in yellow.**

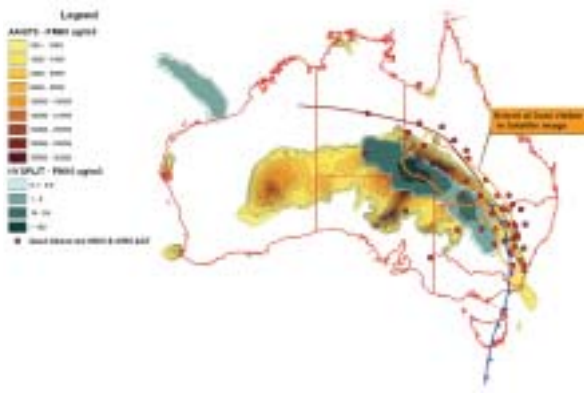

Forecasts valid 2000 UTC 22 October 2002 (0600 EST 23 October)

This forecast comparison is shown in Fig. 13. There are a few apparently extraneous areas of dust in both forecasts but in general both provide a good indication of the location of the dust front when compared with the satellite image and the 2100 UTC (0700 EST) MSLP analysis. The analysis shows the cold front and the pre-frontal trough to be positioned near the leading edge of the dust visible in the satellite imagery with this correspondence being less good towards the northern end of the visible dust cloud. HYSPLIT has again reproduced the shape of the front but now lags behind the true position by approximately 180 kilometres. The extension of the northwestern end of the HYSPLIT plume across the southern Northern Territory appears not to be replicated in the satellite image. However, Alice Springs airport reported dust on the 0600 observation and Tennant Creek in the 0900 report. This would appear to indicate that the extent of the dust is considerably greater than can be viewed in the GMS visible imagery, which has a resolution of 1.25 km per pixel. The dust cloud at this time is over 400 km wide at its northern end and approximately 100 km across at its southern extremity.

The dust produced in northern Western Australia (WA) in the model forecast was not observed in any satellite images although Bureau observations for Mandora in WA did record dust on 23 October, and several stations in the area reported haze over this period. The AAQFS forecast shows better agreement with the position of the leading edge of the dust plume visible in the GMS image, lagging behind by only 100-130 km, but again forecasts a large area of dust over Central Australia where none is visible. The areas of maximum concentration in both forecasts are roughly equivalent, in the southwest corner of Queensland.

Stations that observed dust at 0600 or 0900 are also plotted in Fig. 13. The spatial distribution of the observations follows the general pattern observed in the satellite image. Observation of dust at outlying points, away from the visible extent of dust, reinforces the hypothesis that not all of the dust can be seen in the satellite image.

Forecasts valid 0000 UTC 23 October 2002 (1000 EST 23 October)

Four hours later the dust had moved a further ~150 km in a general northeasterly direction (Fig. 14). The satellite data used for this comparison also came from the MODIS instrument aboard the Terra satellite, and the 'split window' analysis noted earlier was again used. The southeastern extremity of the dust plume had reached the coast by this time, observations of dust being reported from several stations along the NSW coast. There are several small patches of what is apparently dust identified in the satel-

Fig. 14 **HYSPLIT and AAQFS dust forecasts for the forecast based at 0000 UTC 22 October 2002, and valid at 0000 UTC 23 October 2002. The positions of the cold front (blue and the pre-frontal trough (red) from the NMOC analyses are shown, together with the outline of the dust plume from the GMS-5 satellite imagery in yellow.**

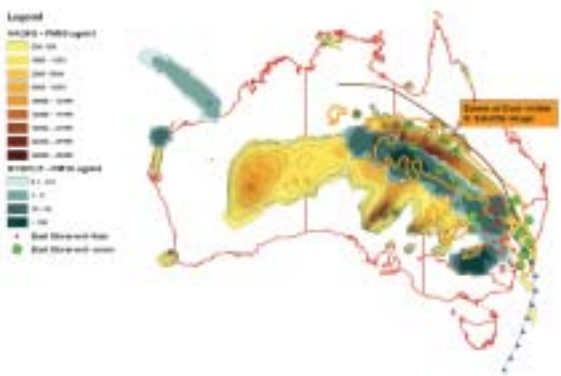

Fig. 15 **HYSPLIT and AAQFS dust forecasts for the forecast based at 0000 UTC 22 October 2002, and valid at 0800 UTC 23 October 2002. The positions of the cold front (blue and the pre-frontal trough (red) from the NMOC analyses are shown, together with the outline of the dust plume from the MODIS satellite imagery in yellow.**

lite image behind the main front. Some coincide with dust observations, one with a high concentration in the HYSPLIT forecast. The Bureau of Meteorology's observation network is not comprehensive enough to conclude that those patches that do not correspond with observations do not actually exist. The HYSPLIT forecast is still aligned closely with analysed position of the cold front but is now some 220 km behind the observed position of the dust front. The AAQFS forecast again provides an excellent forecast of the position of the dust front at this time although also over-forecasting dust to a large degree in both WA and SA.

Forecasts valid 0800 UTC 23 October 2002 (1900 EST 23 October)

The two model forecasts are here compared with the position of the dust front discerned by inspection of a GMS-5 visible image valid at 0800 UTC (Fig. 15). The HYSPLIT forecast over-predicts the dust area, although the general arc-like shape of the plume matches the shape of the cold front/trough line. Dust is being generated along the northwest coast of WA where no dust was observed at this time. The position of the dust front visible in the GMS satellite image does align quite well with the AAQFS forecast, although the AAQFS is also predicting large amounts of dust over the continent.

Discussion

Overall, both models have captured the development and progression of the dust event across the eastern half of the Australian continent. In general HYSPLIT lags behind the observed position of the dust front at all times in these comparisons, while AAQFS better represents the leading edge of the dust cloud in its forecasts, but tends to forecast very large areas of dust. As shown in Fig. 6, strong post-frontal winds were associated with this event, 33-38 kn for several hours after the passage of the front. However, near-surface winds in the LAPS model forecasts were generally less than this, so in many regions where dust was observed model winds were below the designated threshold velocity (10 m s^{-1}) so dust would not be produced. Experiments with lowered threshold velocities (not shown) did move the HYSPLIT forecast dust front into closer alignment with the observations but also generated much larger areas of dust. Positional differences in comparison with AAQFS can be explained by the different methods of initiating dust production within the models. The method used by AAQFS, relying on multiple classifications of vegetation and soils interacting with the meteorological conditions, will almost certainly produce a different spatial and temporal distribution of dust sources than HYSPLIT's simple windspeed related production.

The observation of dust at points close to, but not contained within, the area of dust visible in satellite indicates that the whole extent of the event is probably not being captured by the techniques used here. The over-forecasting of dust by both models indicates that much more attention needs to be paid to dust generation and deposition mechanisms. HYSPLIT is probably most in need of attention but considering the quite simple mechanism currently used, the model has performed well in these comparisons.

The success of both models in replicating the raising of dust and its subsequent transport raises the possibility of producing dust forecasts in real-time. Before this can be achieved with HYSPLIT or AAQFS a more robust mechanism for specifying source areas and dust generation thresholds is required. This should include current values for soil moisture and vegetation cover and possibly land use. During the process of modelling this event it became very evident that a realistic representation of physical variables (e.g. roughness element, geometry, frontal area index), as well as accurate spatial datasets (e.g. leaf area index (LAI), soil type, land use) was required for accurate forecasting. For example AAQFS uses LAI derived from Advanced Very High Resolution Radiometer Normalised Difference Vegetation Index (AVHRR NDVI) data from 1981 to 1994 that does not account for any changes in land use and management that may have occurred more recently. By using different parametrisations of frontal area index (derived from LAI), the forecast amount of dust can differ by 200 to 300 per cent. Reducing LAI itself by 50 per cent (to simulate drought conditions) resulted in an increase in forecast total dust load of 300-500 per cent. These AAQFS sensitivities, and the sensitivity of the HYSPLIT forecasts to two different potential source area specifications, show that these specifications are essential before a robust operational forecast system could be provided.

References

Chan, Y.C., McTainsh, G., Leys, J., McGowan, H. and Tews, K. 2005. Influence of the 23 October 2002 dust storm on the air quality of four Australian cities. *Water, Air, and Soil Pollution 164,* 329-48

Cope, M.E., Hess, G.D., Lee, S., Tory, K., Azzi, M., Carras, J., Lilley, W., Manins, P.C., Nelson, P., Ng, L., Puri, K., Wong, N., Walsh, S. and Young, M. 2004. The Australian Air Quality Forecasting System. Part I: Project description and early outcomes. *Jnl Appl. Met., 43*, 649–62.

Draxler, R.R. and Hess, G.D. 1998. An overview of the HYSPLIT_4 modelling system for trajectories, dispersion and deposition. *Aust. Met. Mag., 47*, 295-308.

Draxler, R.R., Gillette, D.A., Kirkpatrick, J.S. and Heller, J. 2001. Estimating PM10 air concentrations from dust storms in Iraq, Kuwait, and Saudi Arabia. *Atmos. Environ., 35*, 4315-30.

Draxler, R.R. 2004. HYSPLIT4 predicted and measured PM10 air concentrations. Proceedings : *Wind-blown dust workshop*, 8-10 November 2004. CSIRO Atmospheric Research, Aspendale, Victoria Australia,157 pp.

Goudie, A.S. 1983. Dust storms in space and time. *Progress in Physical Geography 7*, 502-30.

Helgren, D.M. and Prospero, J.M. 1987. Wind velocities associated with dust deflation events in the Western Sahara. *Jnl Clim. Appl. Met., 26(9),* 1147-51

Hewson, T.D. 1998. Objective fronts. *Met. Appl. 5*, 37-65.

Lourensz, R.S. and Abe, K. 1983. A dust storm over Melbourne. *Weather, 38*, 272-5.

Loewe F. 1943. Duststorms in Australia. *Bulletin No. 28*, Bur. Met., Australia, 16pp.

Lu, H. and Shao, Y. 2001. Toward quantitative prediction of dust storms: an integrated wind erosion modelling system and its applications. *Env. Modelling & Software, 16*, 233-49.

McTainsh, G.H. 1998. Dust storm index. In *Sustainable agriculture: assessing Australia's recent performance*, Report of the national collaborative programme on indicators for sustainable agriculture, 56-62.

McTainsh, G., Chan, Y., McGowan, H., Leys, J. and Tews, K. 2005. The 23rd October 2002 dust storm in eastern Australia: characteristics and meteorological conditions. *Atmos. Environ., 39*, 1227-36.

McTainsh, G.H. and Pitblado, J.R. 1987. Dust Storms and related phenomena measured from meteorological records in Australia. *Earth Surface Processes and Landforms, 12*, 415-24.

Merrill, J.T., Uematsu, M. and Bleck, R. 1989. Meteorological analysis of long-range transport of mineral aerosols over the North Pacific. *J. Geophys. Res., 94(D6)*, 8584-98.

Middleton, N.J. 1984 Dust storms in Australia: frequency, distribution and seasonality. *Search, 15(1-2)*, 46-7

Mills, G.A. 1997. Studies of cva maxima south of Australia. Part 1: a long-lived enhanced cumulus signature and induced cyclogenesis. *Aust. Met. Mag., 46*, 87-107.

Mills, G.A. 2005. A re-examination of the synoptic and mesoscale meteorology of Ash Wednesday 1983. *Aust. Met. Mag., 54*, 35-55.

Nickling, W.G. 1983. Grain-size characteristics of sediments transported during dust storms. *J. Sedimentary Petrology, 53*, 1011-24.

Pauley, P.M., Baker, N.L. and Barker, E.H. 1996. An observational study of the "Interstate 5" dust storm case. *Bull. Am. Met. Soc., 77*, 693-720.

Puri, K., Dietachmayer, G.D., Mills, G.A., Davidson, N.E., Bowen, R.A. and Logan, L.W. 1998. The new BMRC Limited Area Prediction System. LAPS. *Aust. Met. Mag., 47*, 203-23.

Westphal, D.L., Toon, O.B. and Carlson, T.N. 1987. A two-dimensional numerical investigation of the dynamics and microphysics of Saharan Dust Storms. *J. Geophys. Res., 92*, 3027-9.